Ultrasonic Inspection and Self-Healing of Ge and 3C-SiC Semiconductor Membranes

L. Q. Zhou, G. Colston, M. Myronov, D. R. Leadley, O. Trushkevych, V. Shah, and R. S. Edwards

***Abstract*— Knowledge of the mechanical properties and stability of thin film structures is important for device operation. Potential failures related to crack initiation and growth must be identified early, to enable healing through e.g. annealing. Here, three square suspended membranes, formed from a thin layer of cubic silicon carbide (3C-SiC) or germanium (Ge) on a silicon substrate, were characterised by their response to ultrasonic excitation. The resonant frequencies and mode shapes were measured during thermal cycling over a temperature range of 20–100 °C. The influence of temperature on the stress was explored by comparison with predictions from a model of thermal expansion of the combined membrane and substrate. For an ideal, non-cracked sample the stress and Q-factor behaved as predicted. In contrast, for a 3C-SiC and a Ge membrane that had undergone vibration and thermal cycling to simulate extended use, measurements of the stress and Q-factor showed the presence of damage, with the 3C-SiC membrane subsequently breaking. However, the damaged Ge sample showed an improvement to the resonant behaviour on subsequent heating. Scanning electron microscopy showed that this was due to a self-healing of sub-micrometer cracks, caused by expansion of the germanium layer to form bridges over the cracked regions, with the effect also observable in the ultrasonic inspection. [2020-0017]**

***Index Terms*— Laser ultrasound, vibration, microelectromechanical systems (MEMS), thin films.**

I. Introduction

SOLID thin films are used in a wide variety of engineering systems, including development of micro-electro-mechanical systems (MEMS) and nano-electro-mechanical systems (NEMS) [1]–[4]. The suspended square thin film is a simple MEMS structure and can be used in pressure sensors, or as a platform for integrating devices for applications such as near-infrared photo-detectors, flow sensors, photonic modulators, lasers, and enhancing silicon light emission via carrier injection [5]–[10].

The use of tensile strained membranes, such as Germanium (Ge) on Silicon (Si), can change the electronic or optoelectronic properties by reducing the energy band gap [11], [12]. However, the residual stress in thin films, especially within a multilayer structure, is temperature dependent. Changes in temperature can induce mechanical deformation, which can subsequently lead to damage or failure, influencing the properties of functional devices formed using thin films. Therefore, knowledge of the mechanical properties and stability of the thin film structures at their working temperatures is important. Key threats to the stability of the structures are crack initiation and growth, and delamination between layers, which influence the mechanical reliability. These failure or delamination processes are related to variations in the mechanical interactions between the substrate and thin film layers. In turn, these variations are linked to the residual stress, through processes such as thermal relaxation, in-plane stretching or contraction during operation in an environment subject to vibrational noise, and substrate curvature or plastic yielding [13].

A measurement of the residual stress can be used to determine the risks for cracking and delamination [14]. Recently, several techniques have been used to measure the mechanical stability and residual stress in membranes [15]. These include methods such as curvature measurement and bulge testing [16], [17], X-ray diffraction [18], and resonant vibrational methods [6], [19], [20]. Each technique has advantages and disadvantages [15], [19], but the method of vibrational resonance measurement offers the potential to be developed into a quick, non-destructive method of characterising the properties of membranes during production or in-situ, as well as offering the potential for identification of defects. This technique measures vibration at ultrasonic frequencies, with the resonant frequencies related to the residual stress, and the quality (Q-)factor linked to the membrane quality.

Damage in membranes has been investigated by using techniques such as micro-indentation and stress cycling to produce damage, and is typically measured using a contact profilometer [21]–[23]. In the samples used here, attempts to contact the membrane, for example using atomic force microscopy, have led to breakage. Baumert and Pierron [24] studied Ni structures, measuring the resonant frequency, and showed that this was sensitive to damage, with sudden changes in frequency related to fracture. Chandrahalim *et al.* [25] have studied resonators with frequencies above 1 GHz using laser-Doppler interferometry.

This paper describes vibrational resonance measurements of two types of membrane, for new membranes and those which have undergone extended vibration and thermal cycling to simulate extended use. The measurements offer evidence of the onset of damage, through measurement of several properties including the resonant frequencies (related to residual stress) and the resonance Q-factor. In addition, a Ge film shows evidence of self-healing of sub-micrometer cracks during heating of the membrane, confirmed by microscopy measurements.

Manuscript received February 3, 2020; revised March 6, 2020; accepted March 12, 2020. Date of publication April 1, 2020; date of current version June 2, 2020. This work was supported in part by the Engineering and Physical Sciences Research Council (EPSRC) under Grant EP/F040784/1 and Grant EP/J001074/1, in part by the European Commission (EC) Project under Grant 257375, and in part by the European Research Council (ERC) under Grant 202735. Subject Editor C. Rembe. *(Corresponding author: R. S. Edwards.)*

The authors are with the Department of Physics, University of Warwick, Coventry CV4 7AL, U.K. (e-mail: r.s.edwards@warwick.ac.uk).

Color versions of one or more of the figures in this article are available online at http://ieeexplore.ieee.org.

Digital Object Identifier 10.1109/JMEMS.2020.2981909

TABLE I
REPRESENTATIVE VALUES OF THERMAL EXPANSION COEFFICIENTS OF MATERIALS USED AS SUBSTRATE AND THIN FILM [13]

Material	CTE (10^{-6} °C^{-1})	Temp. range (°C)
Si	3.084 + 0.00196 T	20 to 700
Ge	6.05 + 0.0036 T − 3.5×10^{-7} T^2	20 to 810
3C-SiC	1.6 + 0.0042 (T+273) − 5.9×10^{-7} (T+273)^2	20 to 900

II. RESIDUAL STRESS AND TEMPERATURE

For an ideal tensile-stressed membrane, the relationship between residual stress and the resonant mode frequencies in a vacuum or in air, considering the effect of air damping, is given by

$$f_{mn} = \frac{1}{2}\sqrt{\frac{\sigma}{\rho}\left(\frac{m^2}{l_x^2}+\frac{n^2}{l_y^2}\right)}; \quad f_{air} = \frac{f_{nm}}{\sqrt{(1+\Gamma\beta)}}. \tag{1}$$

Here σ is the biaxial stress, ρ is the film density, l_x and l_y are its lateral dimensions, n & m represent the mode number, $\beta = \rho_{air} l/\rho t$ is the thickness correction factor, ρ_{air} is the density of air, t is the membrane thickness, and Γ is the non-dimensional added virtual mass incremental (NAVMI) factor, which is determined by boundary conditions and mode shape [26]–[29]. The resonance frequency is proportional to the square root of the residual stress; therefore as stress changes, so will the frequency.

The total residual stress σ_T at an arbitrary temperature is governed by two parts: an intrinsic component σ_i which is generated by the lattice mismatch between membrane and substrate during growth [13], [14], and a temperature dependent component σ_{th} which is determined by the coefficients of thermal expansion (CTE) of the membrane and substrate. The total residual stress is given by

$$\sigma_T = \sigma_{th} + \sigma_i, \tag{2}$$

and the thermal component can be approximated as

$$\sigma_{th} = \frac{E}{1-\nu}(\alpha_f(T) - \alpha_s(T))(T_0 - T), \tag{3}$$

where E is the Young's modulus and ν is the Poisson's ratio of the thin film material, and α_f and α_s are the CTE of thin film and substrate [30]. T_0 is the growth temperature of the thin film. The thermal component is taken to be zero during growth, but changes due to contraction or expansion of the thin film and substrate on heating or cooling. A positive value of σ represents tensile stress, while negative is compressive stress [30].

The measurements presented here study two different materials. One type of sample is a Ge suspended thin film with a Si substrate, which will generate compressive stress on the thin film when cooling from the growth temperature to room temperature due to the thermal expansion, because Ge has a larger CTE than Si. The second sample is a cubic silicon carbide (3C-SiC) suspended thin film with a Si substrate, which has the opposite thermal effect to Ge as the sample is cooled from the growth temperature because 3C-SiC has a smaller CTE than Si, with a turning point in measurements of the CTE at a temperature of around 220 °C. The thermal expansion coefficients of thin film and substrate materials are given in table I [13]. Both materials are single crystalline and cubic, 3C-SiC(100) and Ge(100), as confirmed by X-ray diffraction [31]–[33], and can therefore be taken to be isotropic. Mode mixing of modes has been shown to occur on a square membrane, for example modes 2:3 and 3:2 occurring at the same frequency, confirming the isotropic nature of the vibration [6].

TABLE II
SAMPLE LIST

Material	Thickness	Lateral
3C-SiC (damaged)	500 nm	1600 μm
Ge_Sample_1 (damaged)	2 μm	1370 μm
Ge_Sample_2	700 nm	955 μm

III. METHODOLOGY

Ge and 3C-SiC thin films were deposited onto Si substrates by reduced pressure chemical vapour deposition (RP-CVD). Monocrystalline 3C-SiC thin films were grown at high temperature (1100–1200°C) at a pressure of 100 Torr in an ASM Epsilon 2000E RP-CVD system using both a C and Si source precursor. Growth was carried out on 100 mm diameter, on-axis, Si (001) substrates with standard 525 μm thickness. By controlling the growth time, thin film samples with varying thicknesses were achieved. Sample thicknesses can be achieved from tens of nanometers to a few microns, with more information in references [31] and [34].

A two temperature method was used to grow the Ge epitaxial layers. Ge epilayers were also grown within an ASM Epsilon 2000E RP-CVD system on standard Si substrates. The first deposition temperature was 400°C for the first 100 nm thick Ge layer, then the following layer was grown at 670°C, and a final anneal was carried out at a temperature of 830°C for 10 minutes to improve the crystal quality of the Ge epilayer. More growth details are available in references [32], [35], [36].

Both Ge and 3C-SiC epilayers were suspended in the form of square membranes through selective anisotropic wet etching. Photolithography was used to pattern the underside of the Si substrate with Protek PSB, a UV sensitive photoresist resistant to alkaline etchants, giving the required suspended structure geometry [37], [38]. To fabricate the suspended structures, part of the Si substrate was removed using a deep anisotropic wet etching process using 30% tetramethylammonium hydroxide (TMAH) at a temperature between 80 and 90°C for 12-16 hours [31], [39]. Both Ge and 3C-SiC are resistant to etching in TMAH at such temperatures and therefore provide a self-terminating etch process. The etching time depends on the temperature, concentration of chemicals and substrate thickness. The samples presented in this paper are summarised in table II.

The membranes were investigated by measuring their vibrations over a frequency range of 50–500 kHz at a pressure

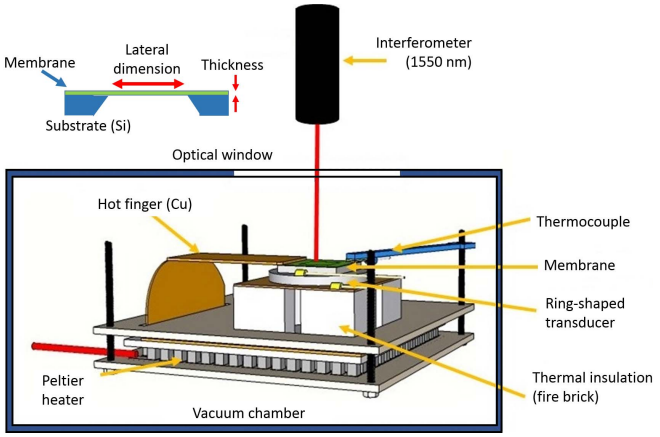

Fig. 1. The measurement set-up used for vibrational testing. The membrane geometry is shown from underneath.

of 10^{-3} mbar, with thermal cycling from 20 to 100 °C to simulate operation at different temperatures over a typical operating temperature range for a semiconductor device. This frequency range was chosen as it includes the fundamental resonance and several higher-order resonances, allowing identification of the fundamental and accurate measurement of the stress. Measurement at a reduced pressure gives a more accurate measurement due to the improved Q-factors and reduction of the impact of the NAVMI. The measurement set-up is shown in figure 1. The membrane was glued to a ring-shaped piezoelectric transducer which was clamped onto an insulated fire brick, also ring shaped and porous, enabling air to be removed equally from both sides of the membrane [20]. The transducer was driven by a function generator with a continuous sinusoidal AC voltage, with the excitation voltage limited to 10 mV to ensure the vibration was in the linear regime [20]. An Intelligent Optical Systems two-wave mixer interferometer was used to measure the membrane's out-of-plane displacement during vibration; this uses a 1550 nm wavelength laser and has a bandwidth of 250 MHz. The laser spot had a diameter of 200 μm. To minimise heating from the laser the power was set to 50 mW; this ensured that any effect from local heating due to the laser was minimal, and this was confirmed prior to testing using thermal imaging.

Measurements of the frequency behaviour of the vibration were taken with the laser at a set of fixed points on the membrane (centre, quarter diagonal, etc.). This ensures that modes with nodes and antinodes in different positions can be measured. The displacement across the membrane was then measured using a 2D scan to identify each mode, with the stress obtained using equation 1 [20]. Temperature cycling was controlled using a Peltier device. Heat was transferred to and from the membrane structure using copper tape to overcome the limited thermal transfer through the transducer. The temperature was measured on the opposite side of the membrane to the hot finger using a Pt1000 resistor with an accuracy of ±0.3 °C. Each measurement was taken once thermal equilibrium had been achieved; thermal imaging was performed at room pressure to ensure that there was no thermal gradient between hot finger and thermal sensor once thermal equilibrium had been reached. All measurements were therefore done after the measured temperature had been stable

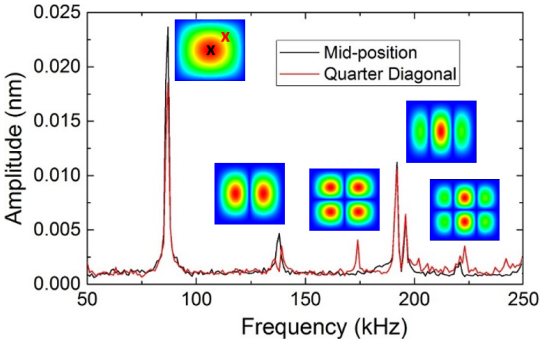

Fig. 2. Frequency scan at two positions on the 3C-SiC membrane. The images show simulated mode shapes for each resonance, with the measurement positions marked on the fundamental.

for at least 30 minutes. A scanning stage was used to enable one- and two-dimensional scanning.

COMSOL was used to model the thermal expansion and its effect on the stress for the Ge film, considering the geometry of the thin film and substrate and their changing dimensions as a function of temperature [40]. Young's modulus was set at 103 GPa, while Poisson's ratio was 0.26. The process was simplified by assuming a single growth temperature, T_0, which is used as the free parameter in equation 3 to fit the experimental data.

IV. Results and Discussion

A. 3C-SiC Thin Film

Figure 2 shows a frequency scan done on the 3C-SiC membrane to identify the resonances, measured at atmospheric pressure. This was done at two positions; close to the membrane centre and on the diagonal, to ensure sensitivity to most modes. The scan was done with a 1 kHz step size. The fundamental resonance mode is around 80 kHz, with higher order resonances at higher frequencies. The stress is related to the frequency of each resonant mode via equation 1, and therefore by using the measured mode frequencies for multiple modes the stress can be obtained. For this sample the stress was found to be 124±1 MPa at room temperature and pressure. This measurement ensures that the fundamental resonance is correctly identified [6], [20].

Following this measurement, the behaviour of the fundamental resonance was measured at 10^{-3} mbar as temperature was changed, with the expected shift in frequency as pressure was reduced. Measurements were performed with the laser at the mid-point of the membrane due to the mode shape and symmetry. Figure 3 shows the results of these measurements. Part (a) plots the magnitude of the vibration at each driving frequency on a colour scale, showing the change in the resonance frequency with temperature, indicating a change in the stress. According to equation 3 and the values of the CTEs in table I, the thermal stress for a 3C-SiC thin film with a Si substrate has a turning point, as the tensile stress becomes compressive stress, at a temperature of around 212 °C. This occurs as the CTE value of 3C-SiC becomes larger than that of Si. Models show that this leads to a peak in the resonant frequency at a temperature of around 120 °C. However, figure 3 shows a reversal of the thermal stress at a much lower temperature than expected, at around 70°C, indicating a mechanism which has released stress.

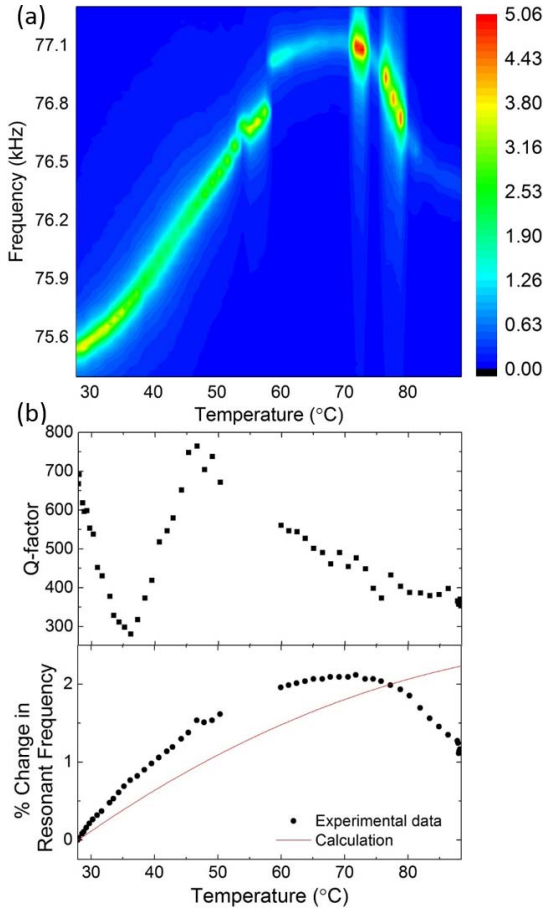

Fig. 3. Results of thermal cycling measurement for the fundamental resonance of 3C-SiC at 10^{-3} mbar. (a) 2D colour map of frequency amplitude response; the colour represents the displacement. (b) Q-factor at resonance, and change in resonance frequency, as a function of temperature. The line shows a calculation using equation 3.

In figure 3(b) the Q-factor for the 3C-SiC film is presented, along with the resonant frequency from the experiment and the calculations. The Q-factor is expected to have two factors influencing the thermal behaviour; as temperature is increased, the glue acting as coupling between transducer and sample softens, which leads to a drop in resonance amplitude above about 40 °C. This softening is beneficial as it ensures that there is no large external force applied due to thermal expansion of the transducer and the sample. In addition, any increase in frequency is linked to an increase in tensile stress, which also affects Q. Here, the Q-factor had an unexpected sharp rise from 36 to 45 °C, which was also observed in measurement of the amplitude of vibration. Following this rise, the effects due to softening of the glue and the change in frequency dominated once more and led to a further reduction in Q-factor.

The jump in the Q-factor and the release of stress are indicative of changes in the boundary conditions of the membrane, potentially due to the initiation of cracking. Unfortunately, this film was sufficiently damaged that it was destroyed, preventing further testing.

B. Ge Thin Films

Two Ge thin films were tested, summarised in table II. One (*Ge_Sample_2*) was a new sample, while *Ge_Sample_1* had undergone prolonged large amplitude vibration.

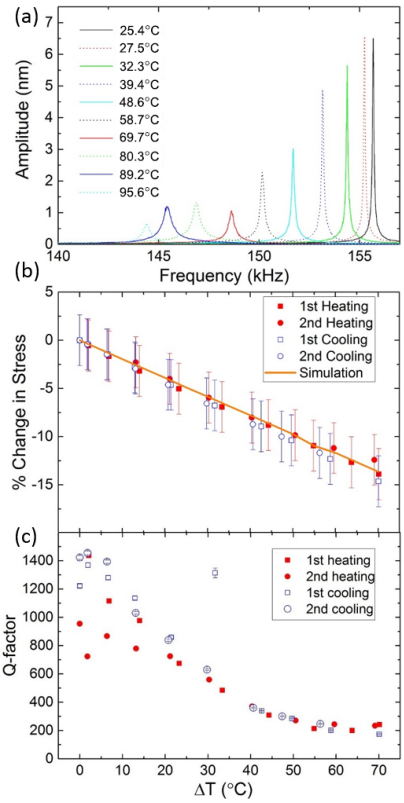

Fig. 4. Measurement of *Ge_Sample_2* at 10^{-3} mbar. (a) Frequency amplitude response (legend gives measurement temperature), (b) percentage change in stress, and (c) Q-factor behaviour. $\Delta T = 0$ is set at room temperature.

Optical microscopy before the thermal cycling tests did not show any damage to either film.

At room temperature and a pressure of 10^{-3} mbar, *Ge_Sample_2* (700 nm thickness and 955 μm lateral dimensions) had a fundamental resonance frequency of 155.33 kHz, and a stress of 0.362 GPa. A value of Γ of 0.40 was found. Figure 4 shows the thermal cycling measurement results. Measurements were again performed with the laser at the mid-point of the membrane due to the mode shape and symmetry of the first resonant mode. The frequency of the fundamental resonance was measured, with results shown in part (a). The resonant frequency drops as temperature is increased, which is linked to a change in stress via equation 2. The percentage change in the stress as the sample is heated ($\Delta T = 0$ is set at room temperature) is shown in (b). The change in stress due to the frequency shift calculated using equation 3 is plotted as a line, using a value of 450 °C for the fit (free parameter T_0). This is a realistic fit parameter compared to the two growth temperatures; the first, low temperature layer will contain most of the defects due to lattice mismatch and dominate the intrinsic stress, while the higher temperature growth layer will show reduced stress. Data is shown for heating and cooling twice from room temperature to the maximum temperature, to show reproducibility. The stress shows a change of approximately 0.2% per °C temperature change, with simulation and results agreeing well.

Figure 4(c) shows the variation in Q-factor as temperature is increased. It is expected that this will drop as temperature

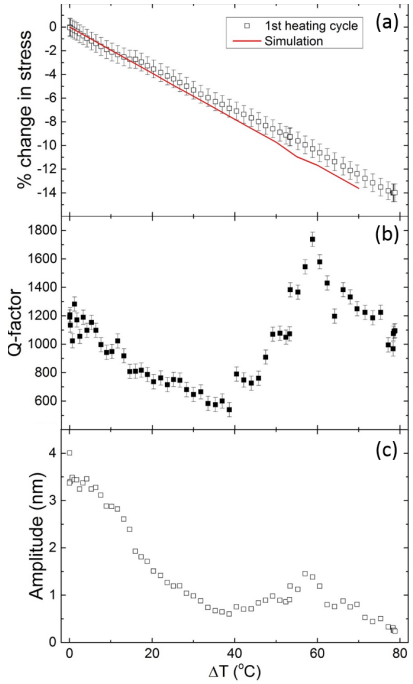

Fig. 5. First heating cycle for *Ge_sample_*1 at 10^{-3} mbar. (a) Shows the percentage change in stress, (b) shows the Q-factor with changing temperature, (c) shows the vibration amplitude at resonance.

is raised, due to the change in stress and frequency, and the variation in coupling between transducer and sample during thermal cycling; the glue softens as temperature is raised, shown by the reduced amplitude in part (a). Any changes in residual stress and boundary conditions will also affect the measurement. A consistent trend of decreasing Q-factor with increasing temperature was observed for all cycles, indicating that any changes for this sample are dominated by coupling variations. At the higher temperatures the effect of the glue softening stabilises, but further reduction is observed due to the change in frequency of the mode.

Figure 5 shows the behaviour of *Ge_sample_*1 (2 μm thickness, 1370 μm lateral dimensions, extended vibration) during its first thermal cycling test. A value of 450 °C was again used for the simulation. At the start of the temperature sweep the stress and Q-factor followed the trends shown in the simulation and for *Ge_sample_*2. However, as temperature increased some variations away from this behaviour were observed. The stress, plotted in figure 5(a), shows variation away from the simulated values above $\Delta T =$ 10 °C, with a change compared to the predictions of the simulation. Similarly, the Q-factor and resonance amplitude (figures 5(b) and (c)) show a sudden increase at $\Delta T = 40$ °C; beyond that point the Q-factor enters a period of growth and then further reduction, indicating a significant change to the thin film at this ΔT followed by resumption of the drop due to changes in frequency and coupling to the transducer. This is similar to the behaviour of the damaged 3C-SiC film, with such changes not observed on *Ge_sample_*2, and hence not attributable to coupling. Alongside the deviation away from the predicted resonance frequency behaviour, this suggests onset of damage to the sample.

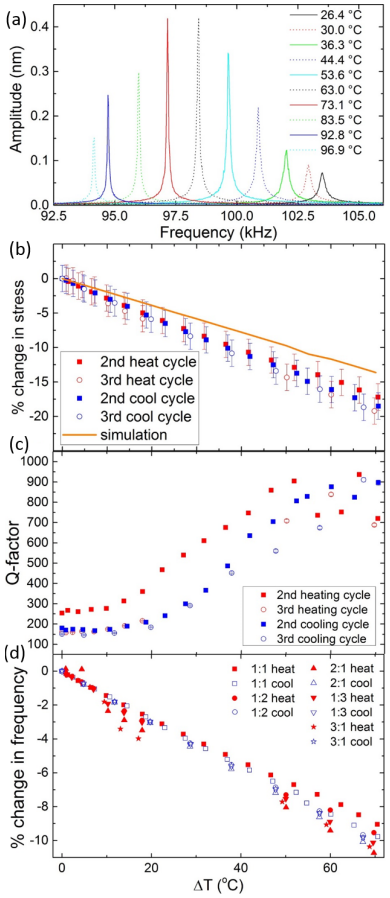

Fig. 6. *Ge_sample_*1, further thermal cycling tests. (a) Frequency response, (b) percentage change in stress found from the fundamental resonance frequency, (c) Q-factor. (d) Shows the percentage change in frequency for several resonant modes.

Sample *Ge_Sample_*1 was then subjected to further thermal cycling, with results shown in figure 6. Part (b) shows the percentage change in stress. Repeatability of the measurements following the changes observed in figure 5 is now found, with the stress changing by 0.28% per °C, which is more than predicted in the simple model over the temperature range observed. The Q-factor shows a cycle and temperature dependent behaviour (figure 6 (c)). There is some small variation in the starting values of the Q-factor at $\Delta T = 0$, but overall the same trend with temperature is observed in each sweep, with the Q-factor increasing with increasing temperature. The behaviour stabilises following the second heating cycle, indicating a stabilisation to changes to the thin film. For a perfect membrane the Q-factor reduces as temperature is increased, primarily due to softening of the coupling between transducer and sample; this increase in Q-factor showed, unexpectedly, an improved resonator as temperature increased. The amplitude response (figure 6 (a)) also displays the opposite behaviour to expectation before a temperature of 73.1 °C; a reduction in amplitude was expected as temperature was increased due to the softening of the coupling, but the rise in amplitude again suggests an improved resonator. The percentage frequency change (and hence stress change) for higher order resonant modes has the same behaviour as found from the fundamental resonance (figure 6 (d)).

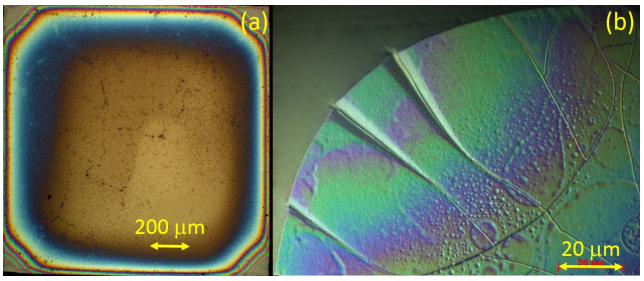

Fig. 7. Microscopy image of *Ge_Sample_*1 (a) before and (b) after the first thermal cycle. (b) Shows the upper left corner of the membrane to show cracking clearly.

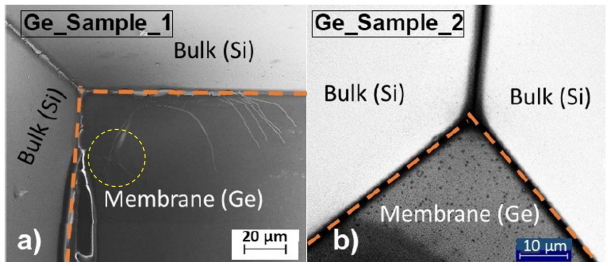

Fig. 8. SEM views from the interface side with Si substrate removed, taken at a corner position at room temperature for (a) sample *Ge_Sample_*1, (b) sample *Ge_Sample_*2. The dashed lines indicate the edges between the suspended Ge and bulk Si. The light lines on the membrane in part (a) are cracks, and the circle indicates the region where the cracking in figure 9(a) and (b) occurs.

The NAVMI Γ can be found by comparing the frequency measured at room pressure and at low pressure. A value of Γ of 0.40 was found for both Ge samples before undergoing heating and cooling cycles. *Ge_Sample_*1 initially had a resonant frequency of 103.09 kHz, corresponding to a stress of 0.228 GPa [20]. Following thermal cycling, the resonant frequency of sample *Ge_Sample_*1 changed to 104.69 kHz, and Γ changed to 0.78. The increased NAVMI factor confirms changing of the boundary conditions, potentially due to cracking. Microscopy measurements confirmed this.

C. Microscopy of Ge Films

To confirm the presence of cracking in *Ge_sample_*1, which showed indications of damage but was still operational as a resonator, microscopy images were taken. Figure 7 shows images taken using an optical microscope. Figure 7 (a) shows the thin film condition before the testing, with no cracks visible. (b) shows a corner of the sample after the first heating cycle, and small cracks can be seen at the corner regions. The diversion from the predicted stress and the change in Q-factor was attributed to this initiation of cracks. The size of the cracks were too small to measure using the optical microscope.

The condition of the two Ge thin films were measured using scanning electron microscopy (SEM, Zeiss SUPRA 55-VP) with preliminary results shown in figure 8. This measured a corner on each of the two thin films, with the image taken from the substrate and interface side. Figure 8(b) shows sample *Ge_Sample_*2 to be a good quality thin film. However, sample *Ge_Sample_*1 shows a series of macroscopic crack-like defects clustered around the membrane edges (figure 8(a)). These are likely due to the previous high amplitude vibrations and thermal cycling, and may have initiated during the

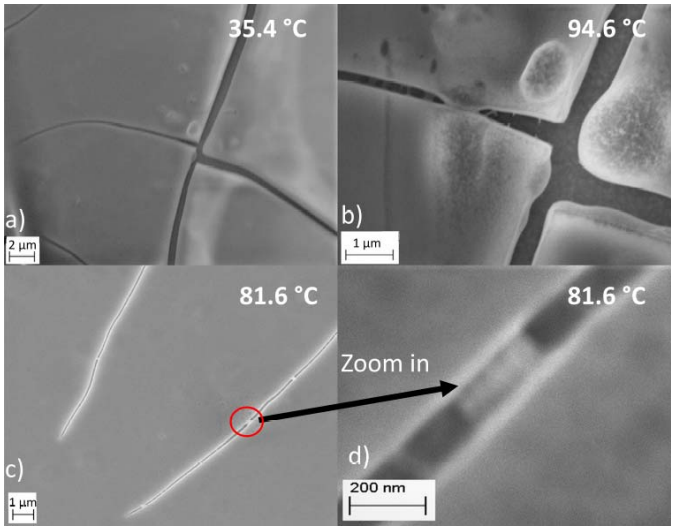

Fig. 9. SEM images of sample *Ge_Sample_*1 taken at 10^{-6} mbar. (a) and (b) Show the same region of the membrane at 35.4 °C and 94.6 °C respectively. (c) and (d) Show another region at 81.6 °C.

measurement shown in figure 5, explaining the change in behaviour of Q-factor, stress and vibration amplitude.

A further SEM measurement utilising temperature control, for a temperature range of 32 to 95 °C, was taken on sample *Ge_Sample_*1 to understand the temperature-dependent behaviour of the stress and Q-factor. The sample was placed on a copper ring, then onto a manually controlled heating stage which replaced the standard sample holder inside the SEM chamber. The resolution of the temperature control stage was 0.1 °C. The SEM chamber pressure was reduced to 10^{-6} mbar. Temperature was measured by a sensor which was fixed inside the copper stage under the sample. Before each measurement the system was left for 30 minutes to reach thermal equilibrium. The measured SEM pictures under different temperatures are shown in figure 9. Part (a) was measured at a temperature of 35.4 °C, part (b) is at the same position as (a) but for a temperature of 94.6 °C, with the image zoomed in to show more detail. Parts (c) and (d) show cracking at another position on the membrane measured at 81.6 °C.

The SEM images under temperature control in figure 9 show interesting thermal behaviour. Parts (a) and (b) show a non-uniform growth and bulging of the Ge, leading to the formation of apparent joins between the two sides of a crack. Similarly, (c) and (d) show a partial bridging of the cracking which appears as the temperature was raised, with multiple bridges observable on both cracks shown in (c). This is due to thermal expansion of the Ge into the cracked region. The depth of the cracks are around 200-400 nm, i.e. less than the thickness of the thin film, hence the non-destructive nature of the cracking and the fact that the thin film was not destroyed. The openings of the cracks range from tens of nm to around 1 μm, with most of the bridges formed when the width was smaller than 500 nm. The cracks at corner positions did not shown any healing as the temperature was increased as they are around 2 to 3 μm wide.

This self-healing phenomenon as the temperature is raised can explain the resonant behaviour and the longevity of the Ge materials during operation. As the temperature is raised

and bridges are formed the thin film resonance behaviour will improve, leading to an increase in Q-factor (as shown in figure 6 (b)), counteracting the reduction in Q due to frequency shifts and temperature dependences in the experimental set-up. This also explains the amplitude increase shown in figure 6(c) for sample *Ge_Sample_*1 as the temperature is increased. The connections improve the propagation of the wave on the thin film, reducing energy dissipation. Crack closure has previously been identified in MEMS materials, but was attributed to oxide growth [22]; this is not the case with these materials.

V. Conclusion

Vibrational resonance measurements of thin films show the potential to be used as a non-destructive testing method to analyse the quality of membranes, either during manufacture or in-situ. This has been demonstrated using membranes which were subject to large amplitude, prolonged vibrations, and thermal cycling, simulating extended use. Changes in thermal expansion of the membrane and the substrate during thermal cycling can lead to damage, which can be enough to destroy the membrane. Cracks can be initiated more quickly when combining large amplitude oscillation and thermal cycling together, both of which may occur in an industrial environment.

Measurement of the resonant behaviour showed the onset of damage through variation of the temperature dependence of the residual stress away from that predicted by a simple model based on the coefficients of thermal expansion of the constituent materials. The Q-factor of the membranes also showed variations, indicative of the onset of damage leading to changes in the boundary conditions of the membranes.

Two healing mechanisms were observed: expansion of the Ge such that the sides of a crack met, and bridging forming from underneath a non-through-thickness crack. This is likely to be the case for sub-micrometer damage, while larger scale damage, or cracks left to grow without any self-healing, will still lead to failure of the device. Thermal annealing is often used to reduce defect densities in Ge, although temperatures are over 1100 K [41]. These temperatures would undoubtedly irreversibly damage device structures, however, it may be possible to partially recover the crystal quality through localised heating techniques such as laser pulse annealing, which is commonly used for dopant activation in semiconductors [42].

Measurement of the resonant behaviour of the membrane offers the potential for a quick, non-destructive technique for measuring the stability of the structures, giving the opportunity to perform annealing. A deviation away from the predicted behaviour of the Q-factor (such as a drop, or a rise with increasing temperature) is indicative of changes to the quality of the membrane, such as the initiation of cracking or onset of self-healing. In addition, unexpected changes in the resonance frequency measured at low pressure are indicative of a change in the NAVMI factor, again related to the mechanical quality of the membrane. Whilst in these measurements piezoelectric transducers were used to activate the sample, there is the potential for using non-contact methods such as optical heating [43] or air-coupled ultrasound transducers, which could be incorporated into a production line, giving a fully non-contact measurement.

Acknowledgment

All data is provided in full in the results section of this article.

References

[1] A. Gassenq *et al.*, "1.9% Bi-axial tensile strain in thick germanium suspended membranes fabricated in optical germanium-on-insulator substrates for laser applications," *Appl. Phys. Lett.*, vol. 107, no. 19, pp. 1–5, 2015.

[2] C. Boztug, J. R. Sánchez-Pérez, F. Cavallo, M. G. Lagally, and R. Paiella, "Strained-germanium nanostructures for infrared photonics," *ACS Nano*, vol. 8, no. 4, pp. 3136–3151, Apr. 2014.

[3] Y. Ishikawa, "Ge/SiGe for silicon photonics," *Proc. SPIE*, vol. 10131, Jan. 2017, Art. no. 101310C.

[4] K. Wada, "Electronics and photonics convergence on Si CMOS platform," *Proc. SPIE*, vol. 5357, pp. 16–24, Jul. 2004, doi: 10.1117/12.533807.

[5] J. R. Jain, A. Hryciw, T. M. Baer, D. A. Miller, M. L. Brongersma, R. T. Howe, "A micromachining-based technology for enhancing germanium light emission via tensile strain," *Nature Photon.*, vol. 6, no. 6, pp. 398–405, May 2012.

[6] O. Trushkevych *et al.*, "Laser-vibrometric ultrasonic characterization of resonant modes and quality factors of ge membranes," *Sci. Technol. Adv. Mater.*, vol. 15, no. 2, Apr. 2014, Art. no. 025004.

[7] V. A. Shah *et al.*, "Flat single crystal Ge membranes for sensors and opto-electronic integrated circuitry," *Solid-State Electron.*, vol. 98, pp. 93–98, Aug. 2014.

[8] S. Saito, A. Z. Al-Attili, K. Oda, and Y. Ishikawa, "Towards monolithic integration of germanium light sources on silicon chips," *Semicond. Sci. Technol.*, vol. 31, no. 4, Apr. 2016, Art. no. 043002.

[9] H. Mao *et al.*, "MEMS-based tunable Fabry–Perot filters for adaptive multispectral thermal imaging," *J. Microelectromech. Syst.*, vol. 25, no. 1, pp. 227–235, Feb. 2016.

[10] K. Xu *et al.*, "Light emission from a poly-silicon device with carrier injection engineering," *Mater. Sci. Eng., B*, vol. 231, pp. 28–31, May 2018.

[11] M. El Kurdi *et al.*, "Control of direct band gap emission of bulk germanium by mechanical tensile strain," *Appl. Phys.Lett.*, vol. 96, no. 4, 2010, Art. no. 041909.

[12] R. Paiella, C. Boztug, J. Sanchez-Perez, J. Yin, and M. G. Lagally, "Tensilely strained germanium nanomembranes for direct-bandgap infrared light emission," in *Proc. Act. Photonic Mater. VI*, Sep. 2014, p. 91621.

[13] B. L. Freund and S. Suresh, *Thin Film Materials Stress, Defect Formation and Surface Eolution*. Cambridge, U.K.: Cambridge Univ. Press, 2004. pp. 220–309.

[14] J. Auersperg, C. Collet, T. Dean, D. Vogel, and T. Winkler, "Effects of residual stresses on cracking and delamination risks of an avionics MEMS pressure sensor," *Microelectron. Rel.*, vol. 100, no. 64, pp. 665–668, 2016.

[15] K.-S. Chen and K.-S. Ou, "MEMS residual stress characterization: Methodology and perspective," in *Handbook of Silicon Based MEMS Materials and Technologies*, 2nd ed. Amsterdam, The Netherlands: Elsevier, 2010, pp. 305–316.

[16] S. Markutsya, C. Jiang, Y. Pikus, and V. V. Tsukruk, "Freely suspended layer-by-layer nanomembranes: Testing micromechanical properties," *Adv. Funct. Mater.*, vol. 15, no. 5, pp. 771–780, May 2005.

[17] G. C. A. M. Janssen, M. M. Abdalla, F. van Keulen, B. R. Pujada, and B. van Venrooy, "Celebrating the 100th anniversary of the stoney equation for film stress: Developments from polycrystalline steel strips to single crystal silicon wafers," *Thin Solid Films*, vol. 517, no. 6, pp. 1858–1867, Jan. 2009.

[18] U. Welzel, J. Ligot, P. Lamparter, A. C. Vermeulen, and E. J. Mittemeijer, "Stress analysis of polycrystalline thin films and surface regions by X-ray diffraction," *J. Appl. Crystallogr.*, vol. 38, no. 1, pp. 1–29, Feb. 2005.

[19] S. Ma, S. Wang, F. Iacopi, and H. Huang, "A resonant method for determining the residual stress and elastic modulus of a thin film," *Appl. Phys. Lett.*, vol. 103, no. 3, Jul. 2013, Art. no. 031603.

[20] L. Q. Zhou *et al.*, "Non-linear vibrational response of ge and SiC membranes," *Appl. Phys. Lett.*, vol. 111, no. 1, Jul. 2017, Art. no. 011904.

[21] P. Binkhoff, B. Burchard, and D. Hackstein, "Micro-deflection methodology for series production tests of MEMS pressure sensors," *J. Microelectromech. Syst.*, vol. 26, no. 2, pp. 344–350, Apr. 2017.

[22] W. W. Van Arsdell and S. B. Brown, "Subcritical crack growth in silicon MEMS," *J. Microelectromech. Syst.*, vol. 8, no. 3, pp. 319–327, 1999.
[23] H. D. Espinosa and B. Peng, "A new methodology to investigate fracture toughness of freestanding MEMS and advanced materials in thin film form," *J. Microelectromech. Syst.*, vol. 14, no. 1, pp. 153–159, Feb. 2005.
[24] E. K. Baumert and O. N. Pierron, "Fatigue degradation properties of LIGA ni films using kilohertz microresonators," *J. Microelectromech. Syst.*, vol. 22, no. 1, pp. 16–25, Feb. 2013.
[25] H. Chandrahalim *et al.*, "Heterodyne laser-Doppler interferometric characterization of contour-mode resonators above 1 GHz," in *Proc. IEEE Int. Ultrason. Symp.*, Sep. 2009, pp. 1044–1049.
[26] A. Leissa, "Vibration of plates," in *Scientific and Technical Information Division*. Washington, DC, USA: National Aeronautics and Space Administration, 1969.
[27] L. E. Kinsler, A. R. Frey, A. B. Coppens, and J. V. Sanders, *Fundamentals of Acoustics*, 4th ed. Hoboken, NJ, USA: Wiley, 2000, pp. 91–109.
[28] M. K. Kwak, "Hydroelastic vibration of rectangular plates," *J. Appl. Mech.*, vol. 63, no. 1, pp. 110–115, Mar. 1996.
[29] J. Kim, H. J. Kim, E. A. Cho, H. J. Shin, J. H. Park, and K. S. Hwang, "Enhancing the sensitivity of a micro-diaphragm resonating sensor by effectively positioning the mass on the membrane," *Sci. Rep.* vol. 5, pp. 1–8, Oct. 2015.
[30] B. S. Berry, W. C. Pritchet, J. J. Cuomo, C. R. Guarnieri, and S. J. Whitehair, "Internal stress and elasticity of synthetic diamond films," *Appl. Phys. Lett.*, vol. 57, no. 3, pp. 302–303, 1990.
[31] G. Colston, "Wafer scale heteroepitaxy of silicon carbon and silicon carbide thin films and their material properties," Ph.D. dissertation, Dept. Phys., Univ. Warwick, Coventry, U.K., 2018.
[32] V. A. Shah, "Reverse graded high content (x>0.75) Si1-xGex Virtual Substrates," Ph.D. dissertation, Dept. Phys., Univ. Warwick, Coventry, U.K., 2009.
[33] S. D. Rhead *et al.*, "Tensile strain mapping in flat germanium membranes," *Appl. Phys. Lett.*, vol. 104, no. 17, Apr. 2014, Art. no. 172107.
[34] M. Myronov and G. Colston, "Growing expitaxial 3C-SiC on single crystal silicon," U.S. Patent, 013 445 Al, 2017.
[35] J. Halpin, "High quality relaxed germanium layers on silicon," Ph.D. dissertation, Dept. Phys., Univ. Warwick, Coventry, U.K., 2010.
[36] V. A. Shah *et al.*, "High quality single crystal ge nano-membranes for opto-electronic integrated circuitry," *J. Appl. Phys.*, vol. 115, no. 14, Apr. 2014, Art. no. 144307.
[37] M. J. Madou, *Fundamentals of Microfabrication and Nanotechnology: Manufacturing Techniques for Microfabrication and Nanotechnology*, 3rd ed. Boca Raton, FL, USA: CRC Press, 2011, pp. 3–48 & 239–284.
[38] R. C. Jaeger, *Introduction to Microelectronic Fabrication*, 2nd ed. Upper Saddle River, NJ, USA: Prentice-Hall, 2002, pp. 13–21.
[39] I. Zubel and I. Barycka, "Silicon anisotropic etching in alkaline solutions I. The geometric description of figures developed under etching Si(100) in various solutions," *Sens. Actuators A, Phys.*, vol. 70, no. 3, pp. 250–259, Oct. 1998.
[40] *COMSOL Multiphysics Reference Manual, Version 5.0.* [Online]. Available: https://uk.comsol.com/model/thermal-stresses-in-a-layered-plate-273
[41] H.-C. Luan *et al.*, "High-quality ge epilayers on Si with low threading-dislocation densities," *Appl. Phys. Lett.*, vol. 75, no. 19, pp. 2909–2911, Nov. 1999.
[42] R. F. Wood and G. E. Giles, "Macroscopic theory of pulsed-laser annealing. I. thermal transport and melting," *Phys. Rev. B, Condens. Matter*, vol. 23, no. 6, pp. 2923–2942, Mar. 1981.
[43] G. Liu, B. R. Tuttle, and S. Dhar, "Silicon carbide: A unique platform for metal-oxide-semiconductor physics," *Appl. Phys. Rev.*, vol. 2, no. 2, Jun. 2015, Art. no. 021307.